



Cite this: *Polym. Chem.*, 2014, 5, 6811

Injectable hydrogels with *in situ*-forming hydrophobic domains: oligo(D,L-lactide) modified poly(oligoethylene glycol methacrylate) hydrogels†

Niels M. B. Smeets,^a Mathew Patenaude,^a Dennis Kinio,^a Francis M. Yavitt,^a Emilia Bakaic,^a Fei-Chi Yang,^b Maikel Rheinstädter^b and Todd Hoare^{*a}

Injectable, *in situ*-gelling nanostructured hydrogels have been prepared from hydrazide and aldehyde-functionalized polymer precursors based on a copolymer of oligo(ethylene glycol) methacrylate (OEGMA) and an oligo(lactic acid) macromonomer (OLA) with varying lactic acid chain lengths. The resulting hydrogels contain a mix of chemical (hydrazone bond formation between hydrazide and aldehyde groups) and physical (hydrophobic interactions between OLA chains) cross-links which form competitively as a function of the OLA chain length and density. An increase in the OLA chain length and density results in the formation of more physical cross-links and fewer chemical cross-links. Tuning the relative prevalence of physical and chemical cross-link formation facilitated largely independent tuning of gel mechanics relative to gel swelling and degradation. Small-angle neutron scattering of these OLA-containing hydrogels reveals a microstructure consisting of associative hydrophobic domains, based on an increased scattering intensity and decreased blob size relative to that observed for POEGMA hydrogels prepared without the OLA co-monomer. The presence of hydrophobic OLA domains increases the uptake and slows the release of bovine serum albumin, a protein well-known to associate with hydrophobic domains. Coupled with the observed cytocompatibility of the reactive precursor polymers used to prepare the hydrogels, we anticipate significant potential applications of these hydrogels for the prolonged release of hydrophobic cargoes.

Received 10th June 2014,
Accepted 18th August 2014

DOI: 10.1039/c4py00810c

www.rsc.org/polymers

Introduction

Poly(ethylene glycol) (PEG) is a hydrophilic, non-immunogenic and non-cytotoxic polymer that has found wide-spread application in the design of biomaterials for *e.g.* controlled release of therapeutics and tissue regeneration.^{1–4} The use of PEG is particularly attractive as this polymer significantly reduces protein adsorption and consequently cell adhesion, imparting “stealth” capability to mask any underlying biomaterial (*e.g.* nanoparticles,^{5–7} core-shell micelles,^{8,9} polymeric surfaces¹⁰ or even hydrogels^{1,11}) from the host’s immune system.^{5,12,13} From a controlled release perspective, PEG hydrogels have

emerged as potential matrices for release of both small molecule and macromolecular therapeutics given these inherent advantages of PEG-based materials *in vivo*.^{1,11} However, the use of PEG hydrogels in such applications has been limited by their high degree of swelling (and associated limited mechanical strength) and weak drug-hydrogel interactions that result in either fast drug release (in the case of hydrophilic drugs) or poor drug loading (in the case of hydrophobic drugs). Given that conventional PEG hydrogels are prepared from step-growth polymerization of α,ω functionalized PEG macromonomers that cross-link *via* chain ends,^{14–30} chemical modification of the hydrogels to, for example, limit swelling or introduce drug affinity groups to enhance drug-hydrogel interactions is synthetically challenging, at least without sacrificing potential cross-linking sites within the hydrogel that can further exacerbate the challenge of controlling hydrogel swelling.^{27,29} Most of the cross-linking reactions used also result in the formation of non-degradable bonds, making clearance of the hydrogel following use problematic.³¹ As such, while some successful examples of the use of PEG-based hydrogels for delivering

^aDepartment of Chemical Engineering, McMaster University, 1280 Main Street West, Hamilton, Ontario, Canada. E-mail: hoaretr@mcmaster.ca

^bDepartment of Physics and Astronomy, McMaster University, 1280 Main Street West, Hamilton, Ontario, Canada

† Electronic supplementary information (ESI) available: Dynamic light scattering on the POH-OLA precursor solutions. See DOI: 10.1039/c4py00810c

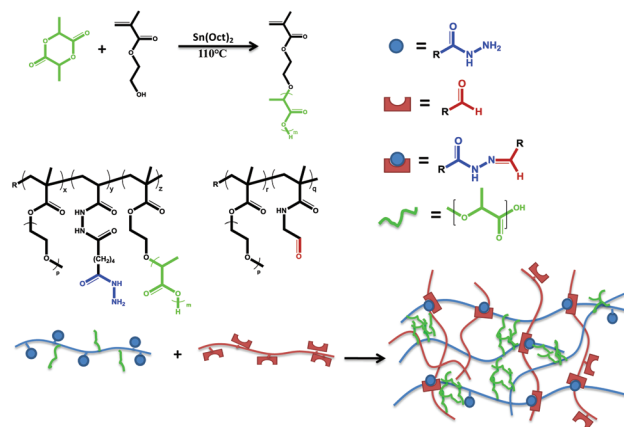
proteins have been reported,^{32–34} the full potential of using PEG-based materials for drug delivery has yet to be unlocked.

The weaknesses of PEG in terms of controlled release applications (*i.e.* degradability and poor bioavailability of hydrophobic therapeutics) can be addressed by combining PEG with hydrophobic, biocompatible, and bioresorbable polymers such as poly(lactic acid) (PLA), poly(glycolic acid), (PGA) or their copolymer poly(lactic acid-*co*-glycolic acid) (PLGA).^{35,36} The design of nanoparticle drug delivery vehicles in particular has benefitted from this approach, wherein PEG-PLA or poly(oligoethylene glycol methacrylate)-PLA (POEGMA-PLA) block copolymers can be assembled into micelles or vesicles that can carry a hydrophobic payload in the hydrophobic PLA core while evading the host's immune system *via* the hydrophilic PEG corona.³⁷ This approach has also been extended to PEG hydrogels through the use of diacrylated PLA-*b*-PEG-*b*-PLA cross-linkers^{38–44} and stereocomplexation between PEG-poly(L-lactic acid) (PEG-PLLA) and PEG-poly(D-lactic acid) (PEG-PDLA) block-copolymers.^{45–48} Recently, Fan and co-workers combined both approaches, using stereocomplexed PLLA and PDLA macromonomers as cross-linkers for hydrogel synthesis.⁴⁹ As a result of their controllable physicochemical properties such as the hydrogel permeability, drug loading, and degradation rate,^{39,41} PEG-PLA hydrogels have been investigated as matrices for controlled release^{40,50} as well as temporary scaffolds for tissue engineering.⁵¹ However, given that the hydrophobic PLA/PGA phase often serves as both the hydrophobic drug depot and the cross-linking site in such hydrogels, independent tuning of cross-link density, drug affinity, and hydrogel degradation in such systems is inherently challenging.

Recently, we have reported the preparation of injectable, *in situ* covalently cross-linked POEGMA hydrogels that display all the desired biointerfacial properties of PEG (*i.e.* protein and cell repellency, non-toxicity, and minimal inflammatory responses *in vivo*).^{52,53} Hydrogel formation occurs through the formation of dynamic covalent hydrazone bonds,^{54,55} which allows for *in vivo* gelation as well as hydrolytic degradation and ultimate clearance of the POEGMA precursors.⁵² Copolymerization of oligo(ethylene glycol methacrylate) monomers (OEGMA) of varying ethylene oxide side chain lengths (*n*) and/or (meth)acrylate monomers with various side chain functionalities allows for facile control over the lower-critical solution temperature (LCST)^{56–58} as well as the functionality of the POEGMA precursors, giving access to POEGMA hydrogels with a broad range of physicochemical properties and drug affinities *via* simple free radical copolymerization.^{52,53}

While these injectable POEGMA hydrogels address many of the challenges associated with PEG hydrogels (degradability, independent control over swelling and mechanical properties, and facile polymer functionalization), hydrogels based on POEGMA have analogous swelling and interfacial properties to PEG hydrogels, making them unlikely candidates to address the issues of fast release of proteins or low uptake of hydrophobic drugs associated with PEG hydrogels.

Herein, we aim to improve the capacity of POEGMA hydrogels for drug delivery by functionalizing hydrogel precursor



Scheme 1 Schematic representation of the synthesis of OLA macromonomers, POH-OLA and POA hydrogel precursors and hydrophobically-modified PO-OLA hydrogels.

polymers with PLA *via* copolymerization of pre-synthesized oligo (*D,L*-lactide) macromonomers (OLA)⁵⁹ with OEGMA during the polymer precursor synthesis (Scheme 1). Our approach differs from most found in the literature given that we do not explicitly use the OLA grafts for the purpose of cross-linking; instead, cross-linking is driven primarily by hydrazone bond formation between the hydrazide and aldehyde-functionalized polymer precursors. As such, the PLA residues will be (at least partially, within the context of the cross-linked network formed) free to self-assemble during gelation *via* hydrophobic association to form a nanostructured hydrogel with nanodomains governed by the mole fraction and side-chain length of the OLA co-monomers. The results show that the incorporated OLA co-monomers significantly alter the physicochemical properties (*i.e.* hydrogel swelling, mechanical strength and degradation) of the POEGMA hydrogels. Furthermore, loading and release of bovine serum albumin (BSA), a model protein which associates with hydrophobic domains,⁶⁰ showed a strong dependence on the mole fraction of PLA in the hydrogel, suggesting that functionalized poly(OEGMA-*co*-OLA) precursors may offer a versatile route towards the synthesis of injectable hydrogels with the potential for sustained release.

Experimental

Materials and methods

Oligo(ethylene glycol) methyl ether methacrylate (OEGMA₄₇₅, Sigma Aldrich, 95%) was purified by passing the monomer through a column of basic aluminum oxide (Sigma Aldrich, type CG-20) to remove the methyl ether hydroquinone (MEHQ) and butylated hydroxytoluene (BHT) inhibitors. 2,2-azobisisobutyric acid dimethyl ester (AIBMe, Wako Chemicals, 98.5%), 2-hydroxyethyl methacrylate (HEMA, Sigma Aldrich, 99%) acrylic acid (AA, Sigma Aldrich, 99%), adipic acid dihydrazide (ADH, Alfa Aesar, 98%), *D,L*-lactide (Sigma Aldrich), tin(II)

2-ethylhexanoate (Sigma Aldrich, 95%), 2-hydroxymethacrylate (Sigma Aldrich, >97%) (*N*'-ethyl-*N*-(3-dimethylaminopropyl)-carbodiimide (EDC, Sigma Aldrich, commercial grade) and thioglycolic acid (TGA, Sigma Aldrich, ≥99.8%) were used as received. *N*-(2,2-dimethoxyethyl)methacrylamide (DMEMAm) was synthesized as reported previously.⁵² For all experiments, Milli-Q grade distilled deionized water (DIW) was used. Dimethyl sulfoxide (DMSO, reagent grade) was purchased from Caledon Laboratory Chemicals (Georgetown, ON). Hydrochloric acid (1 M) was received from LabChem Inc. (Pittsburgh, PA). 3T3 mouse cells were obtained from Cedarlane Laboratories (Burlington, ON). Cell proliferation and recovery media contents including Dulbecco's Modified Eagle Medium-high glucose (DMEM), fetal bovine serum (FBS), horse serum (HS), and penicillin streptomycin (PS) as well as trypsin-EDTA were purchased from Invitrogen Canada (Burlington, ON).

Synthetic procedures

Synthesis of oligo(DL-lactide) macromonomers (OLA). Synthesis of the OLA macromonomers with $m = 4, 8$ and 16 lactide repeat units was carried out according to the method of Ishimoto *et al.*⁵⁹ DL-lactide ($m = 4$: 5 g, 34.7 mmol; $m = 8$: 10 g, 69 mmol; $m = 16$: 20 g, 138 mmol) was placed in a 100 mL one-neck round bottom flask and dried overnight under vacuum. HEMA (2.1 mL, 17.3 mmol) and tin(II) 2-ethylhexanoate (32 μL, 0.1 μmol) were then added to the flask, and the mixture was deoxygenated by a repeated vacuum-nitrogen cycle. Subsequently, the reaction mixture was heated to 110 °C under vacuum for 3 hours with stirring. The crude product was dissolved in anhydrous chloroform and washed with 1 M HCl. The organic phase was then washed with deionized water, isolated, and residual chloroform removed using a rotary evaporator operating under vacuum. Yield varied from 85–90% based on the added amount of DL-lactide. ¹H-NMR (600 MHz, CDCl₃, $m = 8$ monomer): $\delta = 1.38$ – 1.63 ppm (24H, CH-CH₃), $\delta = 1.94$ ppm (3H, CH₂=CCH₃), $\delta = 2.79$ ppm (1H, OH), $\delta = 4.26$ – 4.39 ppm (4H, OCH₂-CH₂), $\delta = 4.39$ – 4.51 ppm (1H, CH-(OH)CH₃), $\delta = 5.08$ – 5.29 ppm (7H, C(=O)-CH), $\delta = 5.58$ ppm (1H, CH₂=C), $\delta = 6.10$ ppm (1H, CH₂=C); longer macromonomers had similar peak positions but different integrations corresponding to their specific length.

Synthesis of hydrazide functionalized poly(oligoethylene glycol methacrylate-co-oligo DL-lactide) (POH-OLA). An extensive synthesis protocol for hydrazide-functionalized POEGMA polymers was reported previously.⁵² Recipes for the hydrazide-functionalized polymers used in this work are given in Table 1 and identified *via* the code POH-OLA _{$m-z$} where m is the theoretical number of lactide repeat units and z is the theoretical mole percentage of the OLA macromonomer incorporated into the polymer. As an example (Table 1, entry POH-OLA₈₋₂₀), AIBMe (37 mg, 0.14 mmol), OEGMA₄₇₅ (2.0 g, 4.2 mmol), OLA ($m = 8$, 1.2 g, 1.7 mmol) and AA (171 μL, 2.49 mmol, corresponding to ~30 mol% in each hydrazide-functionalized copolymer) were all dissolved in dioxane (20 mL). Polymerization was continued for 4 hours at 75 °C, after which the polymer was purified and isolated. Subsequently, the carboxylic acid

Table 1 Chemical synthesis of the POH-OLA hydrazide-functionalized polymers

	m [–]	OEGMA ₄₇₅ [g]	OLA [g]	AA [μL]	AIBMe [mg]
POH	—	4.0	0.0	286	35
POH-OLA ₄₋₁₀	4	2.5	0.37	181	35
POH-OLA ₈₋₁₀	8	2.5	0.62	181	35
POH-OLA ₈₋₂₀	8	2.0	1.20	171	35
POH-OLA ₈₋₃₀	8	1.2	1.32	129	18
POH-OLA ₁₆₋₁₀	16	2.5	1.12	181	35

groups of polymer were converted to hydrazide groups at high yield (~90–95%) *via* the carbodiimide-mediated conjugation of a large excess of adipic acid dihydrazide. The functionalized polymers were purified by dialysis and lyophilized for storage.

Synthesis of poly(oligoethylene glycol methacrylate-co-DMEMAm) (POA). An extensive synthesis protocol for aldehyde-functionalized POEGMA polymers was reported previously.⁵² Briefly, AIBMe (32 mg, 0.14 mmol), OEGMA₄₇₅ (4.00 g, 8.4 mmol), DMEMAm (0.60 g, 3.5 mmol) and TGA (1.0 μL, 0.02 mmol) were dissolved in dioxane (20 mL) and polymerized at 75 °C for 4 hours. Subsequently, the polymer was isolated by rotary evaporation and dissolved in 100 mL 0.5 M HCl for 24 hours to convert the acetals to the reactive aldehydes. The functionalized polymers were purified by dialysis and lyophilized for storage.

Chemical characterization

Aqueous size exclusion chromatography (SEC) was performed using a Waters 515 HPLC pump, Waters 717 Plus autosampler, three Ultrahydrogel columns (30 cm × 7.8 mm i.d.; exclusion limits: 0–3 kDa, 0–50 kDa, 2–300 kDa) and a Waters 2414 refractive index detector. A mobile phase consisting of 0.3 M sodium nitrate and 0.05 M phosphate buffer (pH 7) at a flow rate of 0.8 mL min⁻¹ was used for all polymers analyzed, and the system was calibrated with narrowly-dispersed poly(ethylene glycol) standards ranging from 106 to 584 × 10³ g mol⁻¹ (Waters). ¹H-NMR was performed on a Bruker AVANCE 600 MHz spectrometer using deuterated chloroform as the solvent. The acrylic acid content of the polymers was determined using base-into-acid conductometric titration (ManTech Associates) using 50 mg of polymer dissolved in 50 mL of 1 mM NaCl as the analysis sample and 0.1 M NaOH as the titrant. Particle size analysis and the determination of the critical association concentration were performed using a Brookhaven NanoBrook 90Plus particle size analyzer. Polymer solutions were measured as 150 mg mL⁻¹ and 20 mg mL⁻¹ solutions in PBS at 22 °C using a disposable cuvette. Particle size data reported is based on the intensity average size distribution ($n = 3$). A Variant Cary Bio 100 UV-vis spectrophotometer was used to measure the LCST. The polymers were dissolved at a concentration of 1 mg mL⁻¹ in PBS (pH = 7.4) and the absorbance of the polymer solution was recorded at a wavelength of 500 nm at every 0.5 °C over a temperature range

of 10 °C to 80 °C, with the temperature ramped at a rate of 1 °C min⁻¹.

Critical association concentration (CAC)

The critical association concentration (CAC) was determined by measuring the light scattering intensity as a function of the precursor concentration. Hydrazide functionalized precursor polymer (POH-OLA) solutions ranging from 5 × 10⁻⁵ mg mL⁻¹ (~10⁻⁹ mM) to 20 mg mL⁻¹ (~10⁻³ mM) in 10 mM PBS were prepared and measured at 22 °C using a disposable cuvette. The scattering intensity, expressed as the count rate per second (kcps), was averaged over 3 individual measurements each consisting of 12 runs. The scattering intensity as a function of the precursor concentration is plotted as a log–log plot, where CAC is defined as the intersection of two best linear fits ($R^2 > 0.98$) describing the count rate below and above the CAC. Error bars represent the cumulative error associated with slope and intercept fitting.

Hydrogel preparation

The different POEGMA hydrogels were prepared *via* co-extrusion of hydrazide-functionalized (POH-OLA) and aldehyde-functionalized (POA) precursors dissolved in 10 mM PBS. Both polymer precursor solutions were intimately mixed upon injection using a double barrel syringe fitted with a static mixer at the outlet (Medmix Systems). Hydrogel disks for all *in vitro* testing were prepared by extrusion of the reactive polymer precursors through the double barrel syringe into cylindrical silicone rubber molds (diameter = 7 mm, volume = 300 μL) and incubated at room temperature for at least 12 hours to ensure complete gelation prior to further testing. The gelation time (t_{gel}) was determined using a vial inversion test using 1 min cycles. Complete gelation is defined as the time point where the precursor no longer flows in between cycles.

Hydrogel swelling

The swelling kinetics were determined at 22 °C and 37 °C in 10 mM PBS at pH 7.4. The hydrogels were placed into cell culture inserts that are then placed in a 12-well cell culture plate and completely submerged with PBS (4 mL per well). Hydrogel swelling was monitored until equilibrium swelling was reached (generally ~30 hours) by weighing the hydrogels after gently wicking off any non-absorbed PBS. Subsequently, the hydrogels were resubmerged in a fresh 4 mL of PBS solution until the next data point was collected. Error bars represent the standard deviation of the replicate measurements ($n = 4$).

Degradation kinetics

The relative degradation kinetics of the different hydrogels were determined at 37 °C in 50 mM HCl. The hydrogels were placed into cell culture inserts that were subsequently placed in a 12-well cell culture plate and completely submerged with the HCl solution (4 mL per well). Hydrogel degradation was monitored until the hydrogels had completely degraded by weighing the hydrogels after gently wicking off any

non-absorbed HCl. Subsequently, the hydrogels were resubmerged in fresh 50 mM HCl solution (4 mL per well) until the next data point was collected. Error bars represent the standard deviation of the replicate measurements ($n = 4$).

Hydrogel rheology

The rheological properties of the hydrogels were measured using an ARES rheometer (TA Instruments) operating under parallel-plate geometry with a plate diameter of 7 mm and a plate spacing of 1 mm. Rheological properties were measured by first conducting a strain sweep from 0.1–100% strain at 1 Hz to identify the linear viscoelastic range of the hydrogels. A strain was then selected from the middle of this linear range and set as a constant to perform a frequency sweep from 1 to 100 rad s⁻¹ to measure shear elastic (G') and loss (G'') moduli. All measurements were conducted at 22 °C and in triplicate, with error bars representing the standard deviation of the replicate measurements ($n = 3$).

Small angle neutron scattering (SANS)

SANS experiments were conducted using the 30 m SANS NG3 at the NIST Center for Neutron Research (NCNR), Gaithersburg, MD, USA. Sample-to-detector distances of 1 m, 4 m, and 13 m were used at neutron wavelengths of 6 Å. In addition, lenses were used at a wavelength of 8.4 Å for the 13 m distance. Prior to SANS experiments, precursor solutions were prepared at 150 mg mL⁻¹ in 10 mM phosphate buffered D₂O to facilitate scattering contrast. Hydrogels (~300 μL of hydrogel) were subsequently prepared using a double barrel syringe, directly into a demountable 4.32 × 3.49 × 2.16 cm³ sample cell with an internal gap thickness of 1 mm, requiring Polymers extruded into sample cells were left to completely gel for 12 hours prior to analysis. The low q range data was acquired by counting for 15 minutes using the 13 m detection distance followed by 20 minutes using the 13 m distance with lens. The medium q range was collected using a 4 m detection distance, counting for 5 minutes. The high q range was collected using a 1 m detection distance, counting for 2 minutes. The four ranges of data collected were merged using the NCNR's data reduction tool (DAVE).⁶¹ The individual scattering intensity ($I(q)$) plots (eqn (1)) were fitted using a sum of the Ornstein–Zernike function (eqn (2)) and the squared-Lorentzian (or Debye Bueche) function (eqn (3)), as reported previously for hydrogels,^{62,63} to obtain estimates of the correlation length of the network (ξ) and the characteristic size of inhomogeneities (Ξ).

$$I(q) = \frac{\Delta\rho^2 RT\phi^2}{N_A M_{OS}} \left[\frac{I_{Oz}(0)}{1 + \xi^2 q^2} + \frac{I_{SL}(0)}{(1 + \Xi^2 q^2)^2} \right] \quad (1)$$

$$I_{Oz}(q) = \frac{I_{Oz}(0)}{1 + \xi^2 q^2} \quad (2)$$

$$I_{SL}(q) = \frac{I_{SL}(0)}{(1 + \Xi^2 q^2)^2} \quad (3)$$

In eqn (1)–(3), q is the scattering vector, $I_{Oz}(q)$ the scattering term from the Ornstein–Zernike function, $I_{SL}(q)$ the scattering

term from the squared-Lorentzian function, $\Delta\rho^2$ the scattering length density difference squared, ϕ the volume fraction of the solute, N_A Avogadro's number, R the universal gas constant, T the temperature and M_{OS} the osmotic modulus.

Protein loading

Protein loading was determined by incubating hydrogels in a 500 $\mu\text{g mL}^{-1}$ solution of FITC-BSA at 37 °C in 10 mM PBS (pH 7.4). The hydrogels were placed into cell culture inserts that were subsequently placed in a 12-well cell culture plate and completely submerged with the FITC-BSA solution (4 mL per well). These plates were then covered, placed in an incubator at 37 °C, and shaken for 48 hours in darkness. FITC-BSA drug loading was determined from the difference in fluorescence intensity between the loading solution (500 $\mu\text{g mL}^{-1}$) and the loading solution after 48 hours of incubation, using 495 nm and 519 nm as the excitation and emission wavelengths, respectively. Absorbances were subsequently converted to concentrations using a calibration curve prepared for FITC-BSA at known concentrations ($R^2 = 0.99$). Error bars represent the standard deviation of the replicate measurements ($n = 4$).

Protein release kinetics

Release kinetics were determined by incubating FITC-BSA-loaded hydrogels (described above) in 10 mM PBS at pH = 7.4 at 37 °C (4 mL per well). These plates were incubated at 37 °C in darkness and sampled at pre-determined intervals, with PBS replaced with fresh buffer following every sampling point to maintain infinite sink conditions during the full release time period. Release concentrations were monitored by fluorescence as described above for protein loading. Error bars represent the standard deviation of the replicate measurements ($n = 4$).

In vitro cytotoxicity

The cytocompatibility of polymer precursors (and by extension the hydrogel degradation products) was assessed using a MTT assay. NIH 3T3 fibroblasts were plated at density of 1.0×10^4 cells per well in a 24-well plate and maintained in DMEM media supplemented with 10% FBS and 1% penicillin. Polymer concentrations ranging from 200 to 2000 $\mu\text{g mL}^{-1}$

were transferred into wells with cultured cells and incubated for 24 hours. Cell viability was then characterized using a modified MTT assay. The absorbance of the MTT solution was read using a Biorad microplate reader (model 550) at 570 nm and normalized against a 630 nm baseline to account for non-specific scattering. Error bars represent the standard deviation of the measured cell viability percentages ($n = 4$).

Results and discussion

Synthesis of the OLA macromonomers and hydrogel precursors

Oligo(D,L-lactide) macromonomers (OLA_m) were prepared from the stannous(II) octanoate (Sn(Oct)₂)-catalyzed ring opening polymerization (ROP) of D,L lactide (LA) initiated by 2-hydroxyethyl methacrylate (HEMA)⁵⁹ (Scheme 1). OLA macromonomers with LA chain lengths (m) of $m = 4, 8$ and 16 repeat units were targeted by changing the ratio of LA to HEMA. ¹H-NMR analysis shown in Table 2 confirms that the theoretical and experimental values for m are in good agreement, consistent with prior literature.⁵⁹

The OLA macromonomers were copolymerized with oligo(ethylene glycol methacrylate) (OEGMA₄₇₅) and acrylic acid (AA), and the carboxyl groups of the polymer subsequently functionalized with adipic acid dihydrazide (ADH) using carbodiimide (EDC) coupling⁵² to synthesize hydrazide-functionalized precursors (Scheme 1). The poly(oligoethylene glycol methacrylate-co-adipic acid dihydrazide-co-oligo(D,L-lactide) methacrylate) (POH-OLA_{m-z}) precursors are labelled according to their theoretical OLA chain length ($m = 4, 8$ and 16) and the theoretical mol fraction of OLA grafts in the precursor composition ($z = 10, 20$ and 30 mol%). Characteristic ¹H-NMR (600 MHz in CDCl₃) spectra for POH (= PO₁₀₀H₃₀ from our previous work⁵²) and POH-OLA₈₋₂₀ are shown in Fig. 1, confirming the presence of both hydrazide (peak h, $\delta \sim 9.2$ ppm, NH-NH₂) and OLA (peak o, $\delta = 5.12$ –5.26 ppm, C(O)CH(CH₃)O) groups in the functionalized copolymer.

The degree of OLA macromonomer incorporation varies depending on the OLA side chain length. For precursor polymers synthesized with $z = 10$ mol%, OLA₄ and OLA₈ incorporate

Table 2 Chemical analysis of the hydrogel precursors

	Functionality [–]	m^a [–]	OLA (Theo) ^b [mol%]	OLA (Exp) ^c [mol%]	Hydrazide or aldehyde [mol%]	M_n^d [10 ³ g mol ⁻¹]	D^e [–]	N_f^f [–]	N_{OLA}^g [–]	CAC ^h [10 ⁻⁶ mM]
POH(= PO ₁₀₀ A ₃₀)	Hydrazide	—	0	—	27.2	18.1	2.85	15	—	N/A
POH-OLA ₄₋₁₀	Hydrazide	4.4	10	6.0	27.4	19.0	3.38	16	3	1.9 ± 0.3
POH-OLA ₈₋₁₀	Hydrazide	8.5	10	6.4	27.8	16.6	3.42	12	3	7.2 ± 0.4
POH-OLA ₈₋₂₀	Hydrazide	8.5	20	14.0	28.5	16.7	2.93	11	6	6.4 ± 0.5
POH-OLA ₈₋₃₀	Hydrazide	8.5	30	30.0	28.1	16.3	2.41	11	12	5.5 ± 0.5
POH-OLA ₁₆₋₁₀	Hydrazide	16.8	10	4.5	28.8	27.9	3.38	18	3	2.6 ± 0.2
POA(= PO ₁₀₀ A ₃₀)	Aldehyde	—	—	—	28.1	19.6	2.74	12	—	N/A

^a Average number of LA repeat units in OLA macromonomer as determined from ¹H-NMR. ^b Theoretical OLA mol fraction. ^c Experimental OLA mol fraction as determined from ¹H-NMR. ^d Number-average molecular weight as determined from aqueous SEC. ^e Dispersity. ^f Average number of hydrazide or aldehyde groups per chain. ^g Average number of OLA grafts per chain. ^h Critical association concentration (CAC) as estimated from dynamic light scattering; see ESI Fig. S1–S6.

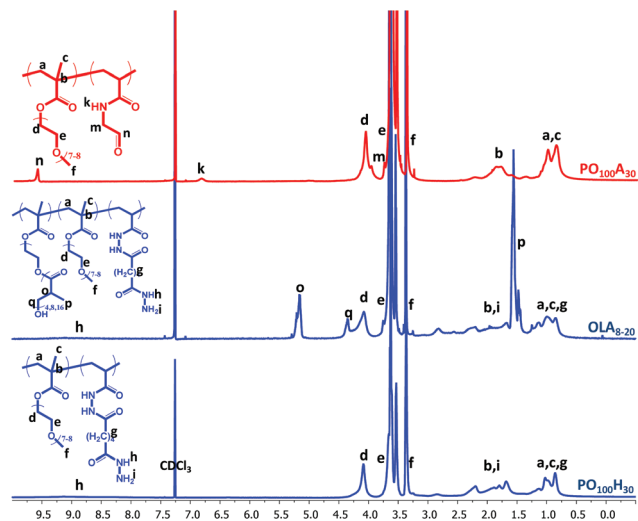


Fig. 1 $^1\text{H-NMR}$ (600 MHz) analysis on the hydrazide, aldehyde and oligo(D,L-lactide) functionalized poly(oligoethylene glycol methacrylate) in CDCl_3 .

to a higher extent than OLA_{16} . The increasing side chain length significantly increases the viscosity of the OLA macromonomer, imposing both diffusional and steric limitations on the copolymerization kinetics. All OLA functionalized precursors have number-average molecular weights (M_n) of $\sim 20 \times 10^3 \text{ g mol}^{-1}$ and relatively broad molecular weight distributions (MWDs) (Table 2). The relatively high values for the dispersity (D) can at least in part be attributed to the fact that size exclusion chromatography (SEC) is performed using linear poly(ethylene glycol) standards whereas the POH-OLA polymers are in reality dense brush copolymers as a result of the long ethylene oxide and lactic acid side chains. The average number of OLA macromonomers incorporated per hydrogel precursor polymer chain (N_{OLA}) was calculated from the OLA mole fraction measured *via* NMR and increases systematically from 3 (for 10 mol% OLA) to 6 (for 20 mol% OLA) to 12 (for 30 mol% OLA), largely independent of the OLA chain length (Table 1). Note that, although OLA_{16} copolymerizes less efficiently when compared to the other macromonomers, the lower degree of incorporation is off-set by the somewhat higher M_n of the POH-OLA₁₆₋₁₀ polymer. Similar to the POH precursor,⁵² none of the POH-OLA precursors display a cloud point or lower-critical solution temperature (LCST) in 10 mM PBS up to 80 °C, despite the contribution of the OLA residues to the hydrophilic-hydrophobic balance of the polymer. Each hydrazide functionalized precursor polymer contains approximately 30 mol% reactive groups, resulting in an approximately equal average number of hydrazide groups per polymer chain (N_f) of 14 ± 3 among all precursor polymers prepared (*i.e.* the number of potential reactive functional groups for cross-linking is approximately equal in each precursor polymer). An aldehyde functionalized poly(oligoethylene glycol methacrylate) precursor POA (= PO₁₀₀A₃₀ from our previous publications⁵²) was synthesized *via* statistical copolymerization of OEGMA₄₇₅ and (*N*-(2,2-dimethoxyethyl)methacrylamide, DMEMAm) followed

by acid catalyzed deprotection of the acetal⁵³ (Scheme 1). The degree of aldehyde functionalization was calculated based on the integrals of the signals at $\delta = 9.58 \text{ ppm}$ (CHO) and $\delta = 3.36 \text{ ppm}$ (O-CH₃) (Fig. 1).

To investigate the solution properties of the precursor polymers, solutions of the hydrazide (POH-OLA_{*m-z*}) and aldehyde (POA) functionalized precursors were prepared at concentrations of 150 mg mL^{-1} in 10 mM PBS (analogous to the pre-gel concentrations to be used). At this concentration, all OLA functionalized precursors yield opaque solutions, which we attribute to aggregate formation driven by hydrophobic interactions between the OLA chains often used to drive macroscopic gelation *via* physical interactions. Self-association of OLA residues would lead to the formation of hydrophobic domains that could serve to (a) supplement the cross-link density of the hydrazone cross-linked hydrogels and (b) facilitate uptake and slow release of hydrophobic drugs or proteins from the hydrogel matrix.

The critical association concentration (CAC) was determined using dynamic light scattering, as previously reported for hydrophobically modified or amphiphilic block copolymers.⁶⁴ POH-OLA precursors yield a marked increase in the scattered light intensity as the precursor concentration is increased from $5 \times 10^{-5} \text{ mg mL}^{-1}$ (10^{-9} mM) to 20 mg mL^{-1} (10^{-3} mM) (Fig. 2). Conversely, the unmodified POH precursor shows only a marginal increase in the scattered light intensity over the same concentration range. The CACs of the POH-OLA precursors are all estimated to be range of $1-7 \times 10^{-6} \text{ mM}$, corresponding to $0.02-0.12 \text{ mg mL}^{-1}$ (Fig. 2). Despite the differences between the POH-OLA precursors, no clear correlation between the CAC and *m* and N_{OLA} was observed, aside from a decrease in CAC as the mole fraction of PLA₈ in the copolymer is increased (Table 2). However, all precursor polymer solutions used for hydrogel formation (150 mg mL^{-1}) lie well above the CAC of all POH-OLA precursors, such that

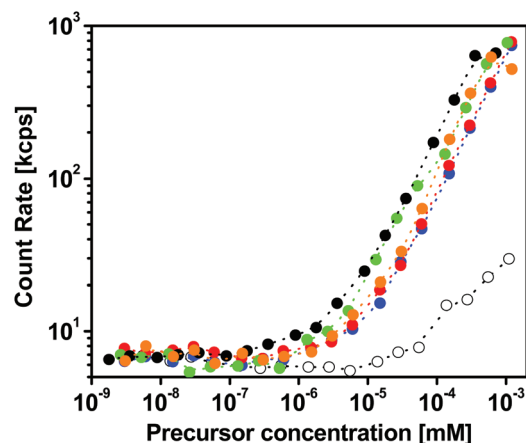


Fig. 2 Scattering intensity of POH-OLA polymers as a function of the polymer concentration in 10 mM PBS as determined from dynamic light scattering. (○, white) POH, (●, blue) POH-OLA₈₋₁₀, (●, red) POH-OLA₈₋₂₀, (●, orange) POH-OLA₁₀₋₃₀, (●, green) POH-OLA₄₋₁₀ and (●, black) POH-OLA₁₆₋₁₀.

hydrophobic domain formation is expected to occur in parallel to covalent gelation of the hydrogels.

Dynamic light scattering experiments on the undiluted precursor solutions (150 mg mL^{-1}) further confirmed the presence of large aggregates in the micron-size range (ESI Fig. S7†); dilution of the precursor solutions to 20 mg mL^{-1} reduced the aggregate size to 100–500 nm (ESI Fig. S8†) but retained a high scattering intensity indicative of a high aggregate concentration. Interestingly, functionalizing the POH-OLA precursors up to 30 mol% OLA ($m = 8$) did not yield macroscopic hydrogels despite the physical aggregation of the precursor polymers observed *via* light scattering.

Hydrogel formation

Hydrazide functionalized POH-OLA and aldehyde functionalized POA precursor solutions (150 mg mL^{-1} , in 10 mM PBS) were co-extruded using a double-barrel syringe to prepare hydrogels. For comparison, a POEGMA hydrogel without any OLA macromonomer was prepared by co-extruding POH and POA. PO-OLA hydrogels were successfully prepared for POH-OLA precursors containing up to 20 mol% OLA. PO-OLA₄₋₁₀ and PO-OLA₈₋₁₀ hydrogels required ~45 min to gel, similar to the unmodified PO hydrogel; PO-OLA_{16,10} and PO-OLA₈₋₂₀ hydrogels gelled in 20 min and 1 h, respectively (see Table 3). In contrast, when POH-OLA₈₋₃₀ was used as the hydrazide-containing precursor polymer, no gelation whatsoever occurred up to 48 hours. This suggests that for a given m , macroscopic gelation becomes progressively slower and is eventually inhibited as the fraction of OLA in the precursor polymers increases, despite the increased hydrophobic associations present. We therefore hypothesize that covalent gelation of these precursor polymers can only occur if the precursor polymers have sufficient mobility following OLA-driven self-assembly to facilitate sufficiently high densities of hydrazone bond formation.

Physicochemical properties of the hydrogels

Hydrogel swelling kinetics were monitored by submerging the PO-OLA hydrogels in 10 mM PBS for 30 hours at 22 °C and 37 °C (Fig. 3). Similar to PEG hydrogels, the POEGMA hydrogel prepared without OLA quickly adsorbs water, reaching an equilibrium mass-based swelling ratio (Q_m) of 18.5 ± 0.5 (at 22 °C) and 16.1 ± 0.0 (at 37 °C) after 6 hours of incubation. In comparison, the OLA containing hydrogels swell considerably

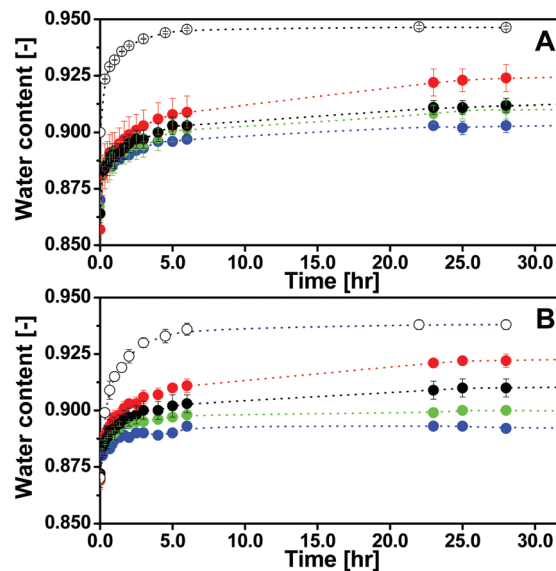


Fig. 3 Swelling kinetics of PO-OLA hydrogels in 10 mM PBS at 22 °C (A) and 37 °C (B). (○, white) PO, (●, blue) PO-OLA₈₋₁₀, (●, red) PO-OLA₈₋₂₀, (●, green) PO-OLA₄₋₁₀, (●, black) PO-OLA₁₆₋₁₀.

slower and reach significantly lower equilibrium Q_m values (Table 3). The lower degree of swelling when compared to the unmodified POEGMA hydrogel may be attributable to the higher hydrophobicity of the hydrogels containing OLA grafts and/or physical cross-link formation within the hydrogel as a result of intermolecular OLA graft interactions. However, the magnitude of the swelling achieved in PO-OLA hydrogels is directly correlated to the overall weight fraction of OLA residues in the hydrogels; PO-OLA₄₋₁₀ and PO-OLA₈₋₁₀ hydrogels contain the lowest weight fraction of OLA (0.95 and 1.57 wt%, respectively, based on the initial hydrogel weight) and reach the lowest Q_m values after swelling for 30 hours while the PO-OLA₈₋₂₀ hydrogel (containing the highest OLA fraction of 3.24 wt%) swells to higher Q_m value. Since the overall hydrophobicity of hydrogels increases with the OLA content (z), this result can only be explained if the effective degree of intermolecular chemical cross-linking is lower in hydrogels prepared with higher OLA contents.

The dynamic hydrazone bond is reversible in aqueous media and in particular in the presence of acidic protons. Hydrogel degradation was evaluated in accelerated conditions in 50 mM HCl to provide comparative degradation profiles

Table 3 Properties of the OLA-functionalized hydrogels (PO-OLA)

	m^a [-]	OLA ^b [wt%]	t_{gel} [min]	Q_m (22 °C) ^c [-]	Q_m (37 °C) ^d [-]	G' [kPa]	ν^e [10^{17} cm^{-3}]
PO	—	0.0	46	18.5 ± 0.5	16.1 ± 0.0	0.52 ± 0.01	1.28 ± 0.02
PO-OLA ₄₋₁₀	4	0.95	55	11.4 ± 0.1	9.9 ± 0.1	0.83 ± 0.07	2.04 ± 0.17
PO-OLA ₈₋₁₀	8	1.57	40	10.4 ± 0.5	9.3 ± 0.2	2.35 ± 0.13	5.79 ± 0.32
PO-OLA ₈₋₂₀	8	3.24	62	15.0 ± 0.7	13.3 ± 0.2	3.37 ± 0.15	8.30 ± 0.37
PO-OLA ₁₆₋₁₀	16	1.72	23	12.2 ± 0.2	11.1 ± 0.2	2.11 ± 0.19	5.20 ± 0.47

All hydrogels prepared by co-extruding 150 mg mL^{-1} precursor solutions in 10 mM PBS. ^a Theoretical OLA chain length. ^b OLA weight fraction in the hydrogels at 22 °C. ^c Volumetric swell ratio measured at 22 °C. ^d Volumetric swell ratio determined at 37 °C. ^e The average cross-link density.

among the different hydrogels prepared (Fig. 4A). Note that both the hydrazone bonds as well as the PLA side-chains can degrade under these conditions, such that both chemical and physical cross-links are expected to be cleaved. The unmodified POEGMA hydrogel initially swells as hydrazone bonds are broken and the cross-link density of the hydrogel decreases. Subsequently, the normalized weight of the hydrogel gradually decreases as polymer chains erode from the bulk hydrogel, with complete degradation of the hydrogel reached within 150 min. With exception of the PO-OLA₈₋₂₀ hydrogel, all PO-OLA hydrogels show similar degradation behaviour and degrade slower than the PO hydrogel, requiring ~240 min to completely degrade (Fig. 4A). This result suggests that the chemical cross-link density for these hydrogels is similar and the variance in OLA graft chain length has little effect on the rate of degradation. For the PO-OLA₈₋₂₀ hydrogel, no initial swelling is observed and the hydrogel degrades rapidly, with complete degradation observed within 45 minutes. This result suggests that the hydrazone cross-link density in PO-OLA₈₋₂₀ is significantly lower than that in the other hydrogels despite the equivalent number of hydrazone reactive functional groups present within the hydrogel precursor solutions between all gels evaluated (Table 2).

The elastic storage modulus (G') and the average number of cross-links per unit volume of hydrogel (ν) were determined from rheological measurements (Fig. 4B and Table 3). Compared to the unmodified PO hydrogel, all PO-OLA hydrogels show higher G' values and, consequently, a higher average degree of cross-linking. Increasing the OLA weight fraction from 0 wt% to 3.24 wt% increases the plateau G' from 0.52 kPa

to 3.37 kPa (Table 3). As the OLA graft chain length increases from $m = 4$ to $m = 8$, G' increases from 2.04 ± 0.17 to 5.20 ± 0.47 kPa due to stronger associations between the OLA grafts at higher m . Increasing m to 16 seems to have little effect on the absolute value of G' ; however, it does alter the shear-dependent rheological behaviour of the gels (Fig. 4B). For example, the G' versus shear frequency profile of a hydrogel prepared with PO-OLA₁₆₋₁₀ (the longest OLA chain used in this work) shows a significant frequency dependence that is absent in gels prepared with shorter OLA chain length macromonomers or without any OLA macromonomers (Fig. 4B). Again, this result indicates that shear-dependent physical cross-links can form in addition to covalent cross-links in the PO-OLA hydrogels, with the number of repeat units in the OLA macromonomer determining the efficacy of intermolecular cross-linking (longer OLA chain lengths, affecting the rheology versus shear) versus intramolecular cross-linking (shorter OLA chain lengths, not impacting the rheology versus shear).

From the results presented in Fig. 3 and 4, we can conclude that cross-linking in PO-OLA hydrogels is combination of two factors: (i) chemical cross-linking through the formation of hydrazone bonds and (ii) physical cross-linking between the hydrophobic OLA grafts. Furthermore, chemical and physical cross-linking in the PO-OLA hydrogels are competing cross-link mechanisms, as the loss of conformational mobility of the polymer chains upon OLA self-association restricts chemical cross-link density. This competing effect is best illustrated by PO-OLA₈₋₂₀, which swells to a higher Q_m (Table 3) and degrades significantly faster than the other hydrogels (Fig. 4A) (*i.e.* it has a lower covalent cross-link density) yet has the highest G' of any tested hydrogel (Fig. 4B) (*i.e.* it has a high physical cross-link density, owing to its highest total mole fraction of LA repeat units among all tested hydrogels as per Table 3). In this way, by exploiting competing cross-link formation mechanisms, hydrogel swelling (Q_m) and mechanical strength (G') can be decoupled, as the physical cross-links add to the mechanical strength but interfere with chemical cross-linking. Increasing the OLA graft density from $N_{OLA} = 3$ to $N_{OLA} = 6$ significantly enhances physical cross-linking and, correspondingly, lowers chemical cross-linking, while increasing the OLA chain length from $m = 4$ to $m = 16$ (at roughly equimolar concentrations) has a minimal effect on the chemical cross-link density (and thus the swelling and degradation kinetics) but increases the plateau modulus of the hydrogel, with longer grafts likely promoting both stronger hydrophobic associations as well as more intermolecular versus intramolecular interactions.

Microstructure of the hydrogels

To support the hypotheses above regarding the effects of the dual chemical/physical cross-linking mechanisms in PO-OLA hydrogels on the hydrogel physicochemical properties, the internal morphologies of the hydrogels were probed. Analogous to the POH-OLA precursor solutions, the PO-OLA hydrogels are translucent and thus show signs of domain formation on a macroscopic scale (insets, Fig. 5). The small angle

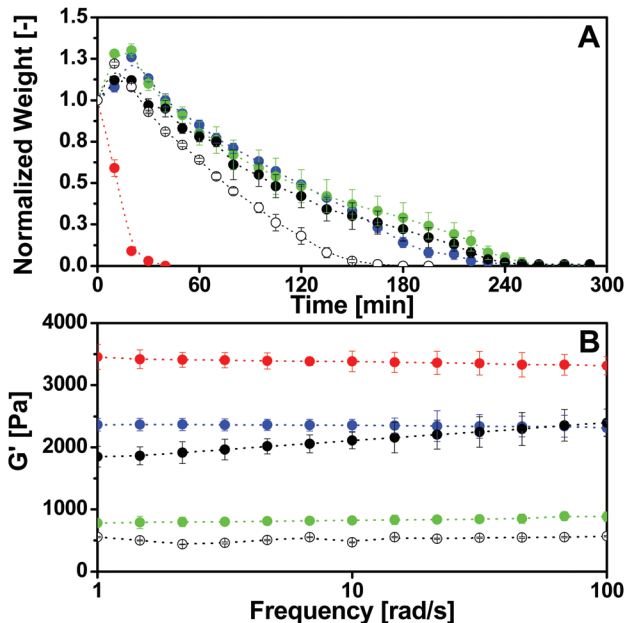


Fig. 4 Degradation kinetics in 50 mM HCl at 37 °C (A) and elastic storage modulus (B) of PO-OLA hydrogels. (○, white) PO, (●, blue) PO-OLA₈₋₁₀, (●, red) PO-OLA₈₋₂₀, (●, green) PO-OLA₄₋₁₀, (●, black) PO-OLA₄₋₁₆, (●, grey) PO-OLA₁₆₋₁₀.

neutron scattering (SANS) intensity functions of the injectable PO-OLA hydrogels prepared at 150 mg mL^{-1} precursor concentration (polymer weight fraction of 0.13 w/w%) are shown in Fig. 5. Comparing the scattering intensity ($I(q)$) results between the different PO-OLA hydrogels (Fig. 5A), structure formation occurs over two different length scales. At the nanometer scale ($\sim 10^{-2} \text{ \AA}^{-1}$ to 10^0 \AA^{-1}), the functions display a broad shoulder; at the micrometer scale ($\sim 10^{-3} \text{ \AA}^{-1}$ to 10^{-2} \AA^{-1}), the functions exhibit a power law scattering regime. Of note, the four PO-OLA hydrogels scatter significantly more at $q < 10^{-2} \text{ \AA}^{-1}$ when compared to the PO hydrogel. A similar increase in $I(q)$ is observed for chemically cross-linked poly (acrylamide) (PAAm) hydrogels with increasing cross-link density.^{65,66} Consequently, the increased scattering at $q < 10^{-2} \text{ \AA}^{-1}$ for the PO-OLA hydrogels suggests the presence of additional cross-linking, likely attributable to hydrophobic associations between the OLA side-chains. The hydrophobic associations add to concentration fluctuations which are 'frozen' into the hydrogel morphology upon random chemical cross-linking.⁶⁷ Concentration fluctuations are likely induced in these hydrogels by the presence of self-assembled polymer aggregates prior to co-extrusion that are subsequently immobilized into the hydrogel *via* covalent cross-linking. The progression in $I(q)$ shows that there is no clear trend in $I(q)$ as a function of the OLA graft content in the hydrogel, likely attributable to the competing effects of chemical and physical cross-linking in these hydrogels described earlier. Interestingly, the PO-OLA₄₋₁₀ and PO-OLA₈₋₂₀ hydrogel SANS functions

show significant structural similarity at $q < 10^{-2} \text{ \AA}^{-1}$ despite indications from the physical gel property measurements that PO-g-OLA₄₋₁₀ is predominantly chemically cross-linked while physical cross-linking dominates in the PO-OLA₈₋₂₀ hydrogel. In comparison, the PO hydrogel that contains no OLA (and thus does not contain hydrophobic domains) scatters significantly less than any of the PO-OLA hydrogels and is thus more homogeneous, as expected.

The correlation length of the network increases with increasing OLA graft density from $20 \pm 0.3 \text{ \AA}$ for PO to $36.8 \pm 0.5 \text{ \AA}$ for PO-OLA₁₆₋₁₀ (Table 4). As the OLA graft density increases, hydrophobic associations between polymer chains promote intramolecular cross-linking that sterically inhibits intermolecular cross-linking and results in an increase in the correlation length of the network.⁶⁸ Correspondingly, the characteristic

Table 4 Structure properties of PO-OLA hydrogels as determined by SANS

	d^a [\AA]	ξ^b [\AA]	Ξ^c [\AA]
PO	110	20.0 ± 0.3	905
PO-OLA ₄₋₁₀	84	19.1 ± 0.4	607
PO-OLA ₈₋₁₀	120	25.7 ± 0.4	531
PO-OLA ₈₋₂₀	86	24.4 ± 0.4	614
PO-OLA ₁₆₋₁₀	175	36.8 ± 0.5	598

^a Average distance between scattering intensities ($d = 2\pi/q$). ^b Correlation length of the network. ^c Characteristic size of network inhomogeneities.

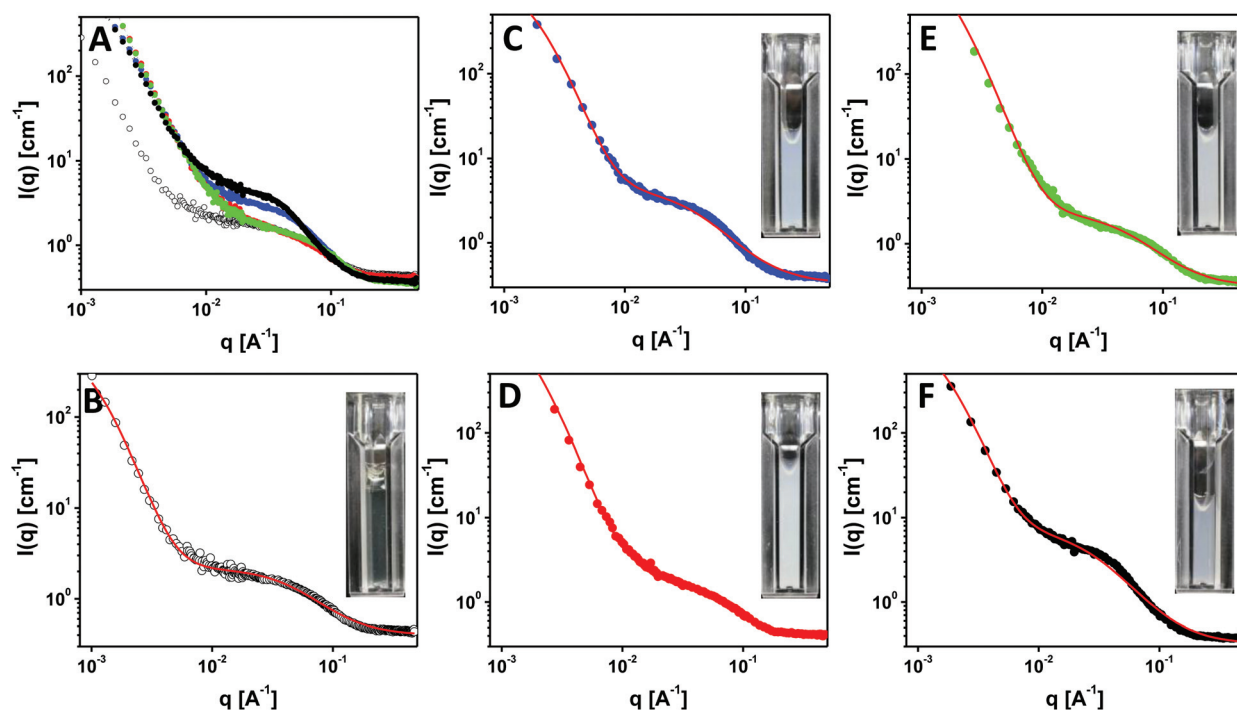


Fig. 5 (A) Small angle neutron scattering (SANS) scattering intensity as a function of the scattering vector (q) for (○, white) PO, (●, blue) PO-OLA₈₋₁₀, (●, red) PO-OLA₈₋₂₀, (●, green) PO-OLA₄₋₁₀, (●, black) PO-OLA₁₆₋₁₀. (B–F) The individual scattering functions (black points) and the fit obtained with the combined Ornstein–Zernike and squared Lorentzian functions (red line) for PO (B), PO-OLA₈₋₁₀ (C), PO-OLA₈₋₂₀ (D), PO-OLA₄₋₁₀ (E) and PO-OLA₁₆₋₁₀ (F). Insets show the optical appearance of the PO-OLA hydrogels prepared at 150 mg mL^{-1} in PBS.

size of inhomogeneities decreases significantly upon the introduction of OLA grafts, from $\bar{\epsilon} = 905 \text{ \AA}$ for PO to $\sim 550\text{--}600 \text{ \AA}$ for the PO-OLA hydrogels. This trend is coupled with an observed decrease in the distance between inhomogeneities from $d = 110 \text{ \AA}$ for the PO hydrogel to $d \sim 85 \text{ \AA}$ for PO-OLA₈₋₂₀ and PO-OLA₄₋₁₀, indicating that the hydrophobic associations between the OLA grafts promote the formation of more and smaller domains. Interestingly, when a longer $m = 16$ graft length is used, the distance between inhomogeneities increases to $d = 175 \text{ \AA}$ while the size of the inhomogeneities remains similar to the other PO-OLA hydrogels; this result suggests the presence of denser domains consistent with the formation stronger hydrophobic interactions. However, there is no clear trend in the size of inhomogeneities between the different PO-OLA hydrogels, likely due to the competing effects of chemical and physical cross-linking in these systems (*i.e.* hydrogels with higher self-associations also have lower covalent cross-link densities).

The indirect evidence of macroscopic structure formation based on the optical appearance (insets Fig. 5), coupled with the SANS analysis (Fig. 5) further suggests the importance of hydrophobic aggregation in defining the microstructure of the PO-OLA hydrogels. Most SANS studies reported thus far on PEG hydrogels focus on chemically cross-linked PEG diacrylates⁶² or physically cross-linked PLA-PEG-PLA triblock-copolymers.⁶⁹ The hydrogel system reported here combines chemical and physical cross-linking, with the physical cross-link density directly influencing the capacity of the polymers to form a covalently cross-linked network.

Drug loading and release

To demonstrate the potential of the PO-OLA hydrogels as injectable hydrogels containing hydrophobic domains for applications in drug delivery, the loading efficiency (Fig. 6) and release kinetics (Fig. 7) of a model protein were determined *in vitro*. Bovine serum albumin (BSA) was chosen as the model protein as it is a moderate molecular weight protein

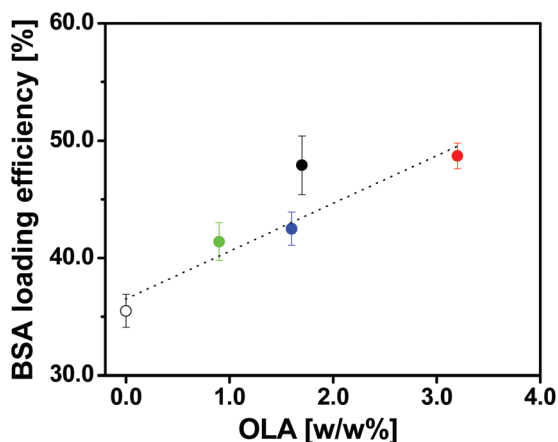


Fig. 6 Bovine serum albumin (BSA) loading efficiency of PO-OLA hydrogels. (○, white) PO, (●, blue) PO-OLA₈₋₁₀, (●, red) PO-OLA₈₋₂₀, (●, green) PO-OLA₄₋₁₀, (●, black) PO-OLA₁₆₋₁₀.

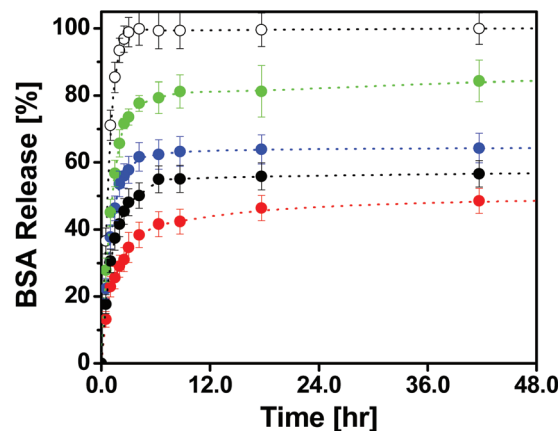


Fig. 7 Cumulative bovine serum albumin (BSA) release over the first 2 days for PO-OLA hydrogels. (○, white) PO, (●, blue) PO-OLA₈₋₁₀, (●, red) PO-OLA₈₋₂₀, (●, green) PO-OLA₄₋₁₀, (●, black) PO-OLA₁₆₋₁₀.

(67 kDa) that is well-known to associate with hydrophobic domains.^{70,71}

BSA partitioning experiments were performed to quantify the affinity of each hydrogel matrix for BSA (Fig. 6). Hydrogels were incubated in a $500 \mu\text{g mL}^{-1}$ BSA solution prepared in 10 mM PBS at $37 \text{ }^\circ\text{C}$ for 48 hours. The unmodified PO hydrogel shows the lowest affinity for BSA, with $35.5 \pm 1.4\%$ of added BSA loaded into the gel phase. The presence of OLA grafts significantly improves the loading efficiency, with the degree of drug uptake increasing linearly with the weight fraction of lactic acid repeat units in the for hydrogels prepared with $m = 4$ and $m = 8$ ($R^2 = 0.979$ for the fit shown in Fig. 6, excluding the black data point for PO-OLA₁₆₋₁₀). The loading efficiency of PO-OLA₁₆₋₁₀, however, is significantly higher than what would be expected based on the weight fraction of OLA in the hydrogel, suggesting that the long OLA chains ($m = 16$) form more hydrophobic domains than the shorter ($m = 4$ and 8) hydrophobic domains (consistent with the SANS data indicating the presence of more compact inhomogeneities with this hydrogel).

BSA release from the loaded PO-OLA hydrogels was subsequently evaluated *in vitro*, with the results shown in Fig. 7. While release is shown only for the first 48 hours for clarity, the plateau values achieved persisted up to 3 weeks of incubation. The unmodified PO hydrogel shows a quick burst release and releases 99% of the loaded amount of BSA in the first 3 hours of incubation. This result is consistent with drug loading experiments that showed that these hydrogels have the lowest affinity for the protein (Fig. 7) as well as the largest degree of swelling (Fig. 3), resulting in a gel matrix with a large mesh size (rapid diffusion) and minimal protein affinity; this is comparable to conventional PEG hydrogels.^{11,72} In comparison, when OLA is incorporated into the hydrogel, a significantly slower burst release is observed over the first 3 hours of incubation and sustained release is achieved following the initial burst, plateauing only after ~ 120 hours (Fig. 7). The magnitude of burst release decreases as the amount of OLA in

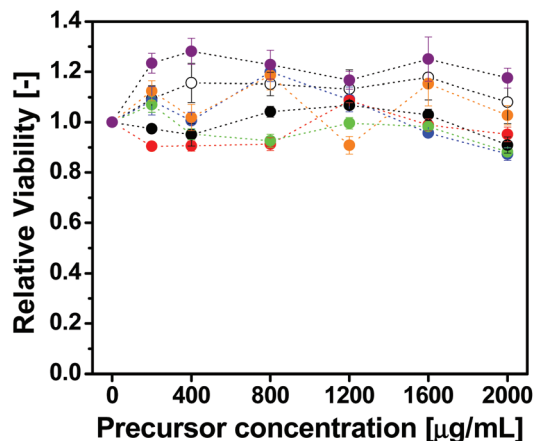


Fig. 8 Cytotoxicity of the polymer precursors and degradation products via MTT assay on 3T3 mouse fibroblasts. (○, white) POH, (●, purple) POA, (●, blue) POH-OLA₈₋₁₀, (●, red) POH-OLA₈₋₂₀, (●, orange) POH-OLA₁₀₋₃₀, (●, green) POH-OLA₄₋₁₀ and (●, black) POH-OLA₁₆₋₁₀.

the hydrogel is increased; as the total weight fraction of OLA was increased from 0.95 wt% (PO-OLA₄₋₁₀) to 3.24 wt% (PO-OLA₈₋₂₀), the burst release over the first 3 hours was decreased from $73.6 \pm 2.4\%$ to $34.6 \pm 4.5\%$. The relative release kinetics are also influenced by the length of the OLA macromonomer, with release rates increasing in the order $m = 4 > m = 8 > m = 16$ for a fixed mole fraction of OLA macromonomer ($z = 10$ mol%). This latter result is consistent with the protein uptake experiments in that the higher affinity hydrogels release protein more slowly. It should also be emphasized that the relative release kinetics cannot be explained solely by swelling differences between the hydrogels; for example, the PO-OLA₈₋₂₀ hydrogel swells the most at 37 °C among the PO-OLA hydrogels (Fig. 3) but shows the slowest drug release kinetics (Fig. 7). Therefore, the difference in release kinetics is primarily attributable to the enhancement in protein–hydrogel interactions due to the presence of hydrophobic OLA side-chains. It is expected that further functionalization of the hydrazide precursor or an increase in the precursor concentration can further improve the drug release kinetics, ultimately aiming towards a minimal burst release followed by long-term sustained release. Furthermore, as neither the POH and POA, nor any of the POH-OLA precursors are cytotoxic up to a concentration of $2000 \mu\text{g mL}^{-1}$ (as determined from a MTT assay on 3T3 mouse fibroblasts, Fig. 8) and the hydrogels are completely degradable (Fig. 4A), these injectable hydrogels offer significant potential for *in vivo* drug release applications.

Conclusions

Oligo(lactic acid) macromonomers have been successfully incorporated into hydrazide-functionalized poly(oligoethylene glycol methacrylate) (POEGMA) reactive precursor polymers to facilitate the formation of injectable PO-OLA hydrogels upon mixing with an aldehyde-functionalized POEGMA precursor.

The resulting hydrogels are cross-linked *via* a combination of chemical (hydrazone bond formation) and physical (OLA side-chain self-association) mechanisms, with the competition between the two mechanisms (*i.e.* increased physical cross-linking results in reduced chemical cross-linking) leading to significant differences in the swelling, mechanical, and degradation properties of the resulting hydrogels. Of particular interest, gel swelling, mechanics, and degradation rate can be independently tuned according to the balance between physical and chemical cross-link formation. Small angle neutron scattering confirms the presence of associative hydrophobic domains inside the hydrogels prepared with OLA macromonomers, with OLA-containing hydrogels exhibiting significantly higher scattering intensities, smaller inhomogeneity sizes, and smaller distances between inhomogeneities relative to hydrogels prepared without OLA macromonomer. The presence of the resulting hydrophobic domains facilitates significantly enhanced loading, reduced burst release, and prolonged sustained release of bovine serum albumin, with protein binding and release directly related to both the length and the density of OLA side-chains present in the hydrogel. Given the *in situ* gelation properties of these materials, the ready tunability of hydrogel properties based on the amount and length of OLA side-chains present, and the degradability of both the chemical and physical cross-linking networks formed within these gels, PO-OLA hydrogels hold significant promise for sustained delivery of hydrophobic or macromolecular therapeutics.

Acknowledgements

Funding from 20/20: NSERC Ophthalmic Materials Research Network, the Ontario Ministry of Research and Innovation Postdoctoral Fellowship program (NMBS) is gratefully acknowledged. We acknowledge the National Institute of Standards and Technology, U.S. Department of Commerce, in providing the neutron research facilities used in this work as well as Dr Boualem Hammouda at NCNR for his assistance with the SANS experiments. Certain commercial equipment, instruments, or materials (or suppliers, or software,...) are identified in this paper to foster understanding. Such identification does not imply recommendation or endorsement by the National Institute of Standards and Technology, nor does it imply that the materials or equipment identified are necessarily the best available for the purpose. Furthermore, we acknowledge Jacqueline Chau for her assistance with critical aggregation concentration measurements.

Notes and references

- 1 C.-C. Lin and K. S. Anseth, *Pharm. Res.*, 2009, **26**, 631–643.
- 2 J. L. Drury and D. J. Mooney, *Biomaterials*, 2003, **24**, 4337–4351.
- 3 N. A. Peppas, J. Z. Hilt, A. Khademhosseini and R. Langer, *Adv. Mater.*, 2006, **18**, 1345–1360.

- 4 B. D. Ratner and S. J. Bryant, *Annu. Rev. Biomed. Eng.*, 2004, **6**, 41–75.
- 5 J. V. Jokerst, T. Lobovkina, R. N. Zare and S. S. Gambhir, *Nanomedicine*, 2011, **6**, 715–728.
- 6 H. Otsuka, Y. Nagasaki and K. Kataoka, *Adv. Drug Delivery Rev.*, 2012, **64**, 246–255.
- 7 U. Wattendorf and H. P. Merkle, *J. Pharm. Sci.*, 2008, **97**, 4655–4669.
- 8 K. Kataoka, A. Harada and Y. Nagasaki, *Adv. Drug Delivery Rev.*, 2012, **64**, 37–48.
- 9 A. Rösler, G. W. M. Vandermeulen and H.-A. Klok, *Adv. Drug Delivery Rev.*, 2012, **64**, 270–279.
- 10 S. Krishnan, C. J. Weinman and C. K. Ober, *J. Mater. Chem.*, 2008, **18**, 3405–3413.
- 11 N. A. Peppas, K. B. Keys, M. Torres-Lugo and A. M. Lowman, *J. Controlled Release*, 1999, **62**, 81–87.
- 12 S. M. Ryan, G. Mantovani, X. Wang, D. M. Haddleton and D. J. Brayden, *Expert Opin. Drug Delivery*, 2008, **5**, 371–383.
- 13 F. M. Veronese, *Biomaterials*, 2001, **22**, 405–417.
- 14 C. R. Nuttelman, M. A. Rice, A. E. Rydholm, C. N. Salinas, D. N. Shah and K. S. Anseth, *Prog. Polym. Sci.*, 2008, **33**, 167–179.
- 15 J. D. McCall and K. S. Anseth, *Biomacromolecules*, 2012, **13**, 2410–2417.
- 16 A. A. Aimetti, A. J. Machen and K. S. Anseth, *Biomaterials*, 2009, **30**, 6048–6054.
- 17 Y. Fu and W. J. Kao, *J. Biomed. Mater. Res., Part A*, 2011, **98**, 201–211.
- 18 M. P. Lutolf and J. A. Hubbell, *Biomacromolecules*, 2003, **4**, 713–722.
- 19 S. P. Zustiak and J. B. Leach, *Biomacromolecules*, 2010, **11**, 1348–1357.
- 20 J. J. Roberts and S. J. Bryant, *Biomaterials*, 2013, **34**, 9969–9979.
- 21 E. A. Phelps, N. O. Enemchukwu, V. F. Fiore, J. C. Sy, N. Murthy, T. a. Sulchek, T. H. Barker and A. J. García, *Adv. Mater.*, 2012, **24**, 64–70.
- 22 M. W. Toepke, N. A. Impellitteri, J. M. Theisen and W. L. Murphy, *Macromol. Mater. Eng.*, 2013, **298**, 699–703.
- 23 N. Cengiz, J. Rao, A. Sanyal and A. Khan, *Chem. Commun.*, 2013, **49**, 11191–11193.
- 24 B. D. Polizzotti, B. D. Fairbanks and K. S. Anseth, *Biomacromolecules*, 2008, **9**, 1084–1087.
- 25 M. Malkoch, R. Vestberg, N. Gupta, L. Mespouille, P. Dubois, A. F. Mason, J. L. Hedrick, Q. Liao, C. W. Frank, K. Kingsbury and C. J. Hawker, *Chem. Commun.*, 2006, 2774–2776.
- 26 R. T. Chen, S. Marchesan, R. A. Evans, K. E. Styan, G. K. Such, A. Postma, K. M. McLean, B. W. Muir and F. Caruso, *Biomacromolecules*, 2012, **13**, 889–895.
- 27 K. C. Koehler, K. S. Anseth and C. N. Bowman, *Biomacromolecules*, 2013, **14**, 538–547.
- 28 D. L. Alge, M. A. Azagarsamy, D. F. Donohue and K. S. Anseth, *Biomacromolecules*, 2013, **14**, 949–953.
- 29 G. N. Grover, J. Lam, T. H. Nguyen, T. Segura and H. D. Maynard, *Biomacromolecules*, 2012, **13**, 3013–3017.
- 30 H. Saito, A. S. Hoffman and H. I. Ogawa, *J. Bioact. Compat. Polym.*, 2007, **22**, 589–601.
- 31 M. Patenaude, N. M. B. Smeets and T. Hoare, *Macromol. Rapid Commun.*, 2014, **35**, 598–617.
- 32 X. Zhao and J. M. Harris, *J. Pharm. Sci.*, 1998, **87**, 1450–1458.
- 33 B. Kim and N. A. Peppas, *Int. J. Pharm.*, 2003, **266**, 29–37.
- 34 J. A. Burdick, M. N. Mason, A. D. Hinman, K. Thorne and K. S. Anseth, *J. Controlled Release*, 2002, **83**, 53–63.
- 35 A. J. R. Lasprilla, G. A. R. Martinez, B. H. Lunelli, A. L. Jardini and R. M. Filho, *Biotechnol. Adv.*, 2012, **30**, 321–328.
- 36 J. M. Anderson and M. S. Shive, *Adv. Drug Delivery Rev.*, 2012, **64**, 72–82.
- 37 J. K. Oh, *Soft Matter*, 2011, **7**, 5096–5108.
- 38 A. S. Sawhney, C. P. Pathak and J. A. Hubbell, *Macromolecules*, 1993, **26**, 581–587.
- 39 A. T. Metters, K. S. Anseth and C. N. Bowman, *Polymer*, 2000, **41**, 3993–4004.
- 40 A. T. Metters, K. S. Anseth and C. N. Bowman, *J. Phys. Chem. B*, 2001, **105**, 8069–8076.
- 41 A. Metters and J. Hubbell, *Biomacromolecules*, 2005, **6**, 290–301.
- 42 K. S. Anseth, A. T. Metters, S. J. Bryant, P. J. Martens, J. H. Elisseeff and C. N. Bowman, *J. Controlled Release*, 2002, **78**, 199–209.
- 43 N. M. Shah, M. D. Pool and A. T. Metters, *Biomacromolecules*, 2006, **7**, 3171–3177.
- 44 I. Barakat, P. Dubois, R. Jérôme, P. Teyssié and E. Goethals, *J. Polym. Sci., Part A: Polym. Chem.*, 1994, **32**, 2099–2110.
- 45 S. J. Buwalda, P. J. Dijkstra and J. Feijen, *Macromol. Chem. Phys.*, 2012, **213**, 766–775.
- 46 S. J. Buwalda, L. Calucci, C. Forte, P. J. Dijkstra and J. Feijen, *Polymer*, 2012, **53**, 2809–2817.
- 47 C. Hiemstra, Z. Zhong, L. Li, P. J. Dijkstra and J. Feijen, *Biomacromolecules*, 2006, **7**, 2790–2795.
- 48 D. G. Abebe and T. Fujiwara, *Biomacromolecules*, 2012, **13**, 1828–1836.
- 49 X. Fan, M. Wang, D. Yuan and C. He, *Langmuir*, 2014, **46**, 14307–14313.
- 50 M. N. Mason, A. T. Metters, C. N. Bowman and K. S. Anseth, *Macromolecules*, 2001, **34**, 4630–4635.
- 51 S. J. Bryant and K. S. Anseth, *J. Biomed. Mater. Res., Part A*, 2003, **64**, 70–79.
- 52 N. M. B. Smeets, E. Bakaic, M. Patenaude and T. Hoare, *Chem. Commun.*, 2014, **50**, 3306–3309.
- 53 N. M. B. Smeets, E. Bakaic, M. Patenaude and T. Hoare, 2014, DOI: 10.1016/j.actbio.2014.05.035.
- 54 A. W. Jackson and D. a. Fulton, *Polym. Chem.*, 2013, 31–45.
- 55 J.-M. Lehn, *Aust. J. Chem.*, 2010, **63**, 611–623.
- 56 J.-F. Lutz, *Adv. Mater.*, 2011, **23**, 2237–2243.
- 57 J.-F. Lutz and A. Hoth, *Macromolecules*, 2006, **39**, 893–896.
- 58 S. Sun and P. Wu, *Macromolecules*, 2013, **46**, 236–246.

- 59 K. Ishimoto, M. Arimoto, T. Okuda, S. Yamaguchi, Y. Aso, H. Ohara, S. Kobayashi, M. Ishii, K. Morita, H. Yamashita and N. Yabuuchi, *Biomacromolecules*, 2012, **13**, 3757–3768.
- 60 Y. An, L. Zhang, S. Xiong, S. Wu, M. Xu and Z. Xu, *Colloids Surf., B*, 2012, **92**, 246–253.
- 61 R. T. Azuah, L. R. Kneller, Y. Qui, P. L. W. Tregenna-Piggott, C. M. Brown, J. R. D. Copley and J. Dimeo, *J. Res. Natl. Inst. Stan. Technol.*, 2009, **114**, 341–358.
- 62 S. Lin-gibson, R. L. Jones, N. R. Washburn and F. Horkay, *Macromolecules*, 2005, 2897–2902.
- 63 T. Matsunaga, T. Sakai, Y. Akagi, U. Chung and M. Shibayama, *Macromolecules*, 2009, **10**, 1344–1351.
- 64 Ö. Topel, B. A. Çakır, L. Budama and N. Hoda, *J. Mol. Liq.*, 2013, **177**, 40–43.
- 65 M. Shibayama, *Macromol. Chem. Phys.*, 1998, **30**, 1–30.
- 66 S. Mallam, F. Horkay, A.-M. Hecht and E. Greissler, *Macromolecules*, 1989, 3356–3361.
- 67 M. Shibayama, *Polym. J.*, 2010, **43**, 18–34.
- 68 N. S. Davidson, R. W. Richards and A. Maconnachiet, *Macromolecules*, 1986, **441**, 434–441.
- 69 S. K. Agrawal, N. Sanabria-Delong, P. R. Jemian, G. N. Tew and S. R. Bhatia, *Langmuir*, 2007, **23**, 5039–5044.
- 70 S. C. Semple, A. Chonn and P. R. Cullis, *Adv. Drug Delivery Rev.*, 1998, **32**, 3–17.
- 71 A. Chonn, S. C. Semple and P. R. Cullis, *J. Biol. Chem.*, 1992, **267**, 18759–18765.
- 72 L. M. Weber, C. G. Lopez and K. S. Anseth, *J. Biomed. Mater. Res., Part A*, 2009, **90**, 720–729.